Vibrational Spectroscopy of Small Hydrated CuOH+ Clusters

ARTICLE *in* THE JOURNAL OF PHYSICAL CHEMISTRY A · FEBRUARY 2014

Impact Factor: 2.69 · DOI: 10.1021/jp411614t · Source: PubMed

3 AUTHORS, INCLUDING:

Jia Zhou
Konkuk University
38 PUBLICATIONS **762** CITATIONS
SEE PROFILE

Etienne Garand
University of Wisconsin–Madison
46 PUBLICATIONS **714** CITATIONS
SEE PROFILE

THE JOURNAL OF PHYSICAL CHEMISTRY A

Article

pubs.acs.org/JPCA

Vibrational Spectroscopy of Small Hydrated $CuOH^+$ Clusters

Brett M. Marsh, Jia Zhou, and Etienne Garand*

Department of Chemistry, University of Wisconsin, 1101 University Avenue, Madison, Wisconsin 53706, United States

Supporting Information

ABSTRACT: Coordinated copper hydroxide centers can play an important role in copper catalyzed water oxidation reactions. To have a better understanding of the interactions involved in these complexes, we studied the vibrational spectra of D_2 tagged $CuOH^+(H_2O)_n$ clusters in the OH stretch region. These clusters are generated by electrospray ionization and probed via cryogenic ion vibrational spectroscopy. The results show that the copper center in the $n = 3$ clusters has a distorted square planar geometry. The coordination in $CuOH^+(H_2O)_n$ is therefore more akin to $Cu^{2+}(H_2O)_n$ with four ligands in the first solvation shell than $Cu^+(H_2O)_n$ with two ligands in the first solvation shell. There is also no evidence of any strong axial ligand interactions. The well-resolved experimental spectra enabled us to point out some discrepancies in the calculated spectra, which were found to be highly dependent on the level of theory used.

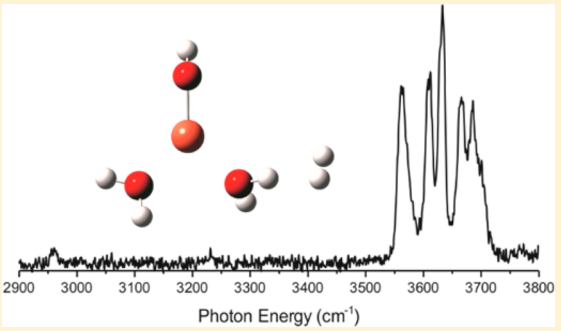

I. INTRODUCTION

Copper is an earth-abundant metal with a ubiquitous presence in homogeneous and heterogeneous catalysis. It also plays crucial roles in the field of biological oxygen chemistry. The versatility and reactivity of copper chemistry make it an appealing candidate for the development of rationally designed catalysts.[1] Very recently, several studies have found examples of coordinated copper complexes catalyzing water oxidation.[2−4] In one instance, the electrocatalytic water oxidation is driven by Cu(II) salts in a basic buffer solution, where the buffer anions coordinate to Cu(II) to prevent it from precipitating out of the solution.[2,5] In the other two studies, the Cu(II) center is coordinated with polypeptide and bipyridine ligands.[3,4] These catalytic systems are robust, simple to assemble, and have good reactivity. In all of these cases, the active species is thought to be a coordinated $CuOH^+$ core.

An important aspect of copper chemistry is its coordination with ligands and its solvation dynamics, which involve a combination of electrostatic, covalent, and hydrogen bonds. Understanding these interactions is necessary to understand and predict the reactivity of copper catalysts. In this respect, gas phase ion vibrational spectroscopy has proven to be one of the most powerful techniques in providing structural and bonding information on well-defined systems.[6−9] Here we use electrospray ionization to isolate microsolvated $CuOH^+\cdot(H_2O)_n$ (n = 1−3) clusters and study their structure and bonding by monitoring the spectral features in the OH stretching region.

Solvated copper systems have been subjected to several mass spectrometry studies. The sequential binding energies of H_2O molecules to Cu^+ have been determined via collision induced dissociation experiments.[10,11] The solvation of Cu^{2+} ions was also studied via dissociation mass spectrometry.[12−16] Furthermore, infrared photodissociation spectroscopy was applied to the study of $Cu^+(H_2O)_n$[17−19] and $Cu^{2+}(H_2O)_n$,[20] yielding vibrational spectra that provided new insights into the coordination and solvation structure around the copper cation. One system that is rarely studied is the $CuOH^+\cdot(H_2O)_n$ complex. The interaction of the OH ligand and H_2O ligand creates an extra layer of complexity in the solvation dynamics. In one study, it was shown that the $CuOH^+\cdot(H_2O)$ loses an OH upon collisionally activated decomposition at low collision energy, whereas $CuOH^+\cdot(H_2O)_2$ loses an H_2O.[16] The second H_2O appears to bind more weakly to the copper and brings to question whether the $CuOH^+\cdot(H_2O)_n$ complex would have a coordination number of 2, similar to $Cu^+(H_2O)_n$,[19] or a coordination number of 4, similar to $Cu^{2+}(H_2O)_n$.[20] Furthermore, with increasing attention paid to copper as a possible water oxidation catalyst, it is important to have a good understanding of the competing Cu−OH and Cu−H_2O interactions, as they may play crucial roles in the catalytic cycle.

In the present paper, $CuOH^+\cdot(H_2O)_n$ (n = 1−3) clusters are studied via cryogenic ion vibrational spectroscopy. The OH stretch modes, which are used as a sensitive probe of the solvation network,[21] are monitored as a function of cluster size. Cryogenic cooling required for D_2 tagging also resulted in IR spectra that are relatively simple and well-resolved. This greatly facilitates comparison with electronic structure calculations and allows for unambiguous assignment of the observed features. The experimental data also highlight some shortcomings of various calculation methods in application to this open-shell system.

Received: November 26, 2013
Revised: February 24, 2014
Published: February 25, 2014

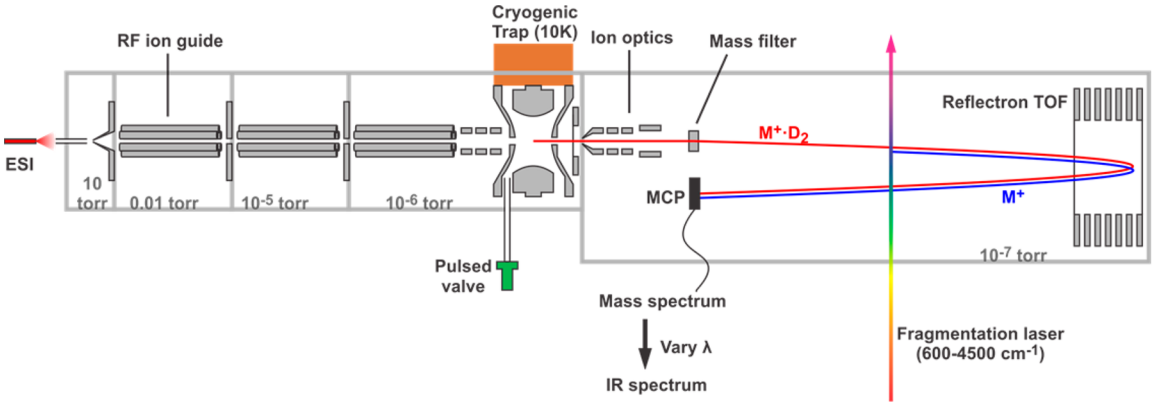

Figure 1. Schematic of the cryogenic ion vibrational spectrometer setup, which combines an electrospray source, a cryogenic quadrupole ion trap, and a reflectron time-of-flight photofragmention spectrometer.

II. EXPERIMENTAL AND THEORETICAL DETAILS

The experiments were carried out in a home-built cryogenic ion vibrational spectrometer based on an improved version of the design by Kamrath et al.[22] The apparatus combines an electrospray ionization source[23,24] to directly transfer fragile ions from solution into the gas phase, a cryogenically cooled ion trap[22,25,26] to cool and tag the ions, and a reflectron time-of-flight photofragmentation spectrometer[27] to separate and detect the photofragments. The schematic of the apparatus is shown in Figure 1.

The $CuOH^+\cdot(H_2O)_n$ complexes were formed by the electrospray ionization (ESI) source, using a 1 mM solution of $CuSO_4$ in water. The ESI tip was held at ~2 kV, and the capillary potential was ~100 V. Three sets of radio frequency (RF) hexapole ion guides, powered by home-built self-oscillating RF supplies based on the O'Connor design,[28,29] brought the ions across three differentially pumped regions. In the main chamber, the ions were accumulated, stored and collisionally cooled in a 3D quadrupole ion trap (Jordan TOF, Inc.) attached to the second stage of a closed-cycle helium cryostat (Sumitomo) and held at 10 K through resistive heating. The trapping buffer gas, composed of 10% D_2 in a balance of helium, was introduced in a short burst (~1 ms) via an external pulsed valve. The trap storage time was adjusted between 50 and 95 ms to optimize the condensation of D_2 molecules onto the cold ions. The accumulated D_2-tagged ions were extracted directly into a reflectron time-of-flight mass spectrometer (Jordan TOF, Inc.) by shutting down the trap RF voltage and applying opposite voltages to the trap end-cap electrodes. The ions of interest were isolated by a gating deflector, and intersected by the output of an Nd:YAG pumped OPO/OPA infrared laser (Laservision). The parent and photofragment ions were separated by a two-stage reflectron and detected by a microchannel plate. The IR spectra were obtained by monitoring the intensity of the photofragment ion as a function of the photon energy.

Geometry optimization and vibrational frequency calculations for the $CuOH^+\cdot(H_2O)_n$ species in their doublet ground state were carried out using the cam-B3LYP, MP2 and CCSD methods and the TZVP basis set. Zero-point energy corrections were taken into account for the calculation of binding energies. For comparison with experimental spectra, the calculated harmonic frequencies obtained by each method were scaled by a factor of 0.953, 0.946, and 0.946, respectively. These values are obtained by comparing the calculated stretch frequencies of an isolated H_2O molecule with experimental values of 3657 and 3756 cm^{-1}. All the calculations were carried out using the Gaussian 09 program.[30]

III. RESULTS

A typical positive mode mass spectrum (1 mM $CuSO_4$ in water) is shown in panel A of Figure 2. Each doublet pair

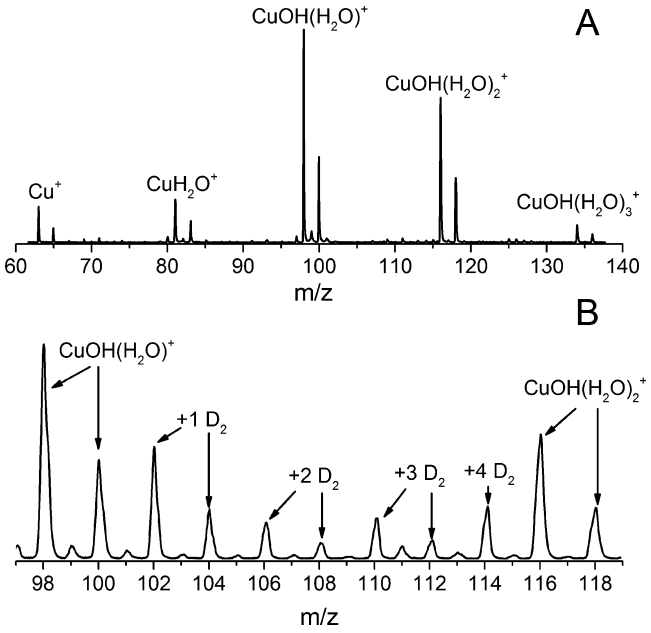

Figure 2. (A) Mass spectrum obtained by ESI of a 1 mM $CuSO_4$ solution in water. (B) Mass spectrum of D_2-tagging of $CuOH^+\cdot(H_2O)$ obtained when the ion trap temperature is held at 10 K.

corresponds to the ^{63}Cu and ^{65}Cu isotopes of copper, reflecting their natural abundances. The two lowest mass doublets are assigned to the bare Cu^+ and $Cu^+\cdot(H_2O)$. The three subsequent doublets are the $CuOH^+\cdot(H_2O)_n$ (n = 1−3) species of interest. There is also very small amount of $CuO^+\cdot(H_2O)$ and $Cu^+\cdot(H_2O)_2$, which are visible around the two $CuOH^+\cdot(H_2O)$ peaks. Interestingly, very little bare $CuOH^+$ is present in the mass spectrum. Vukomanovic and Stone[16] have reported a very similar mass spectrum from the ESI of a similar $CuSO_4$ solution and showed that $Cu^+(H_2O)$ is the dominant fragmentation product of the $CuOH^+\cdot(H_2O)$ cluster at low collisional energies. The intensities we observe in our mass

dx.doi.org/10.1021/jp411614t | J. Phys. Chem. A 2014, 118, 2063−2071

spectrum are in agreement with this result. When the ion trap temperature is lowered to 10 K, D_2 molecules condense onto the clusters, and further complex formation can be observed in the mass spectrum, as shown in Figure 2B. In this specific mass range, the clustering of D_2 molecules onto $CuOH^+\cdot(H_2O)$ forms ions tagged with up to four D_2, with larger clusters overlapping in mass with $CuOH^+\cdot(H_2O)_2$. The distribution of the tagged species was found to be very sensitive to experimental conditions such as the kinetic energy of the ions entering the trap and the pressure of buffer gas in the trap. This behavior is similar to what was observed in other cryogenic ion trap H_2 condensation studies.[22,31] The distribution of tagged species is therefore more representative of the ion cooling and condensation kinetics in the trap than the relative stability of certain tagging numbers. Typical photofragmentation mass spectra obtained when the laser frequency is on/off resonance are shown in Figure S1 (Supporting Information).

An overview of the infrared predissociation spectra of $CuOH^+\cdot(H_2O)_n$ with n = 1−3 in the 2600−3800 cm^{-1} range is presented in Figure 3. These spectra were acquired by monitoring the loss of D_2 from the corresponding singly tagged $CuOH^+\cdot(H_2O)_n\cdot D_2$ ions. The spectral features are concentrated in the free−OH region between 3550 and 3750 cm^{-1}. Specifically, Figure 3A shows the spectrum of the n = 1 species, with three main peaks at 3590, 3612, and 3684 cm^{-1}, as well as a weaker feature at 3758 cm^{-1}. These features have a full width at half-maximum (fwhm) of 20−25 cm^{-1}, and they are

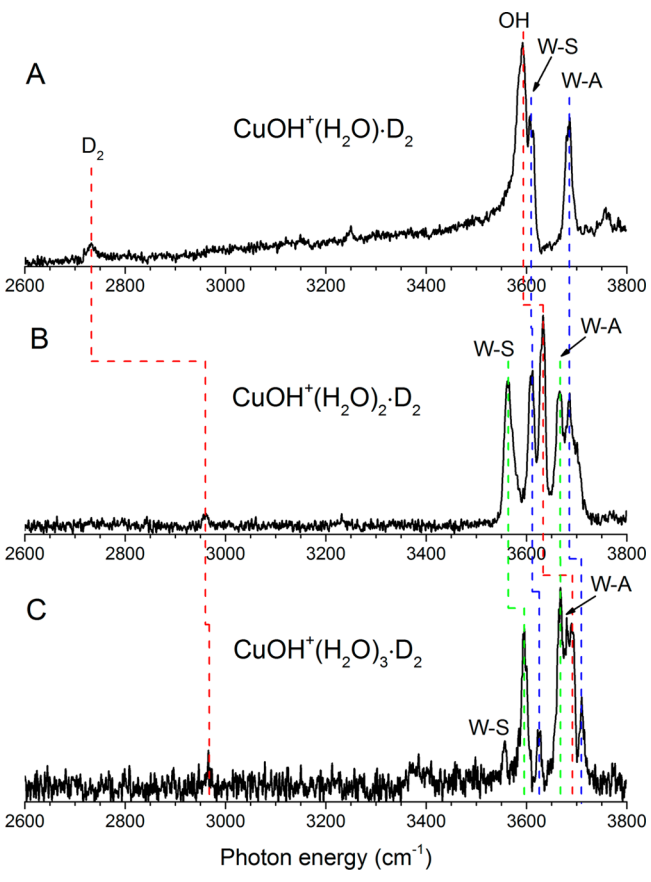

Figure 3. Overview of the infrared predissociation spectrum of (A) $CuOH^+\cdot(H_2O)\cdot D_2$, (B) $CuOH^+\cdot(H_2O)_2\cdot D_2$, and (C) $CuOH^+\cdot(H_2O)_3\cdot D_2$. W-S denotes symmetric stretch of water, W-A denotes antisymmetric stretch of water.

on top of a slowly increasing background starting at ∼2900 cm^{-1} with a dip at ∼3600 cm^{-1} between the two partially resolved peaks.The spectrum is featureless below 3550 cm^{-1}, except for a small peak at 2733 cm^{-1}. The spectrum of the n = 2 cluster, shown in Figure 3B, displays five distinct peaks of similar intensities centered at 3565, 3610, 3632, 3665, and 3685 cm^{-1}. These features are slightly sharper than those in the n = 1 spectrum, with a fwhm of 15−20 cm^{-1}. A weak peak at 2960 cm^{-1} is also visible. Figure 3C shows the spectrum of the n = 3 species. The resolved peaks in this spectrum have the narrowest widths of about 10 cm^{-1} fwhm. The more intense peak at 3595 cm^{-1} is surrounded by two weaker features at 3556 and 3625 cm^{-1}. The broad feature at ∼3680 cm^{-1} can be fitted nicely with three Gaussian peaks centered at 3667, 3681, and 3692 cm^{-1} with fwhm of around 10 cm^{-1}. Lastly, the peak to the blue of the broad feature is situated at 3710 cm^{-1}.

Shown in Figure 4 is a series of spectra corresponding to increasing number of D_2 tags on the $CuOH^+\cdot(H_2O)$ cluster, acquired to probe the perturbation caused by the D_2 tag at different binding sites. These spectra were obtained by monitoring the fragment corresponding to the loss of all tags. These results are particularly relevant for the small cluster because the under-coordinated open-shell metal center in this cluster might be reactive toward hydrogen. As can be seen from Figure 4, the sequential addition of D_2 molecules causes some noticeable changes in the IR spectrum. All four spectra show a common feature at 3590−3609 cm^{-1}, whereas the two other

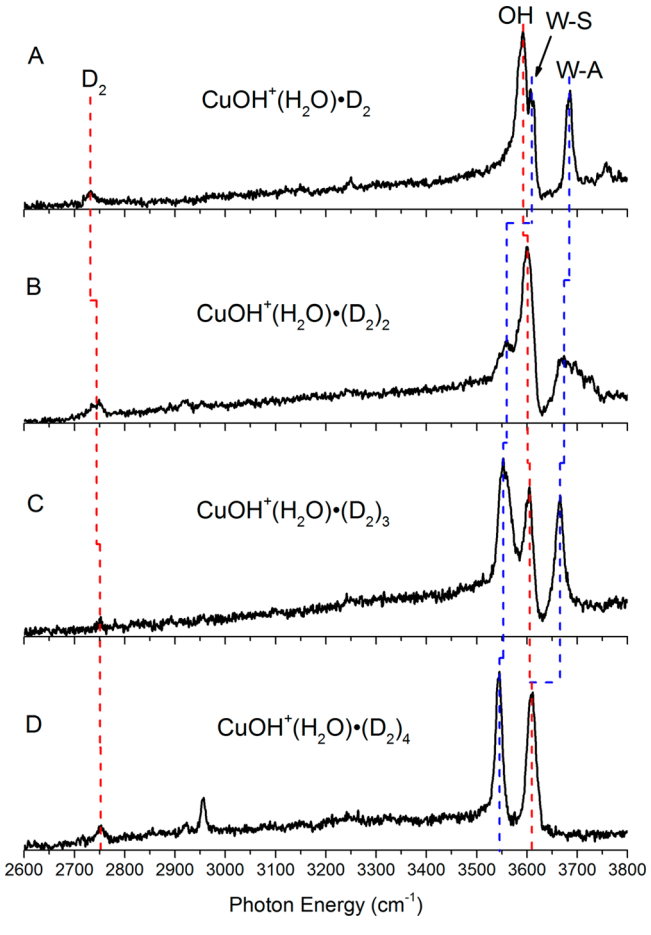

Figure 4. Overview of the infrared predissociation spectrum of $CuOH^+\cdot(H_2O)$ with 1−4 D_2 tags.

dx.doi.org/10.1021/jp411614t | J. Phys. Chem. A 2014, 118, 2063−2071

peaks gradually red shift as the number of tags is increased. They move from 3612 and 3684 cm^{-1} to 3544 and 3609 cm^{-1}, respectively, assuming that the bluest feature in the 4-tags spectrum consists of two overlapping peaks. The very weak feature at around 2750 cm^{-1} is present at about the same frequency for all four spectra, and a new stronger feature appears at 2956 cm^{-1} in the 4-tags spectrum.

IV. DISCUSSION

To have a better understanding of the coordination around the copper core, the effect of D_2 tagging on the observed vibrational frequencies, and the ability of electronic structure calculations to accurately predict structures and IR spectra, we start with a detailed analysis of the spectra of the $CuOH^+\cdot(H_2O)$ cluster with 1−4 D_2 tags presented in Figure 4.

The cam-B3LYP/TZVP optimized geometry of the lowest energy $CuOH^+\cdot(H_2O)$ structure is shown in Figure 5C. The

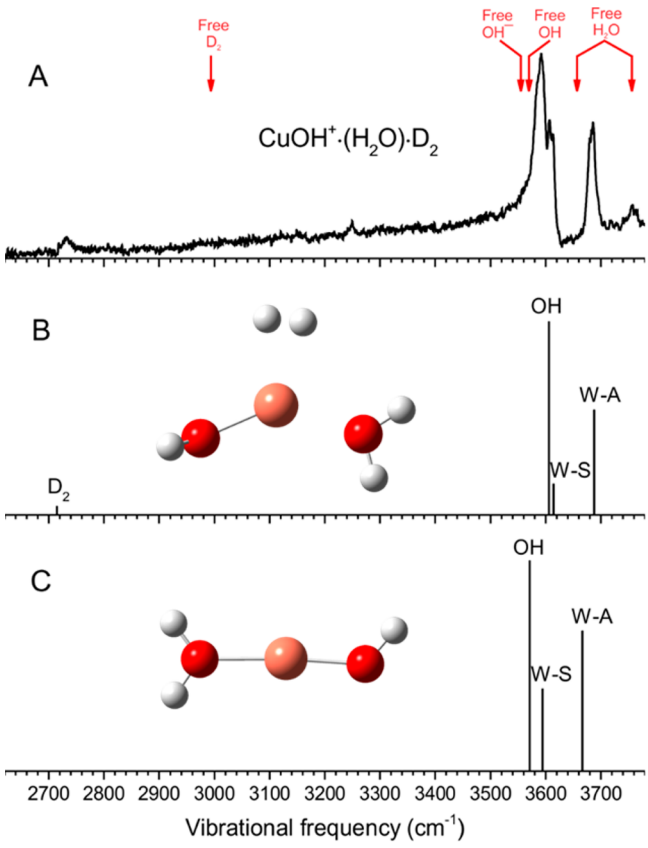

Figure 5. (A) Experimental spectra of $CuOH^+\cdot(H_2O)\cdot D_2$. The red arrows indicate the gas phase positions of each free species. (B) and (C) Vibrations and optimized geometry of $CuOH^+\cdot(H_2O)\cdot D_2$ and $CuOH^+\cdot(H_2O)$ obtained at the cam-B3LYP/TZVP level.

water and hydroxide bind opposite of each other, forming an almost linear O−Cu−O bond with all the hydrogen atoms in the same plane. Two other possible isomers involving a second solvation shell were also found and shown in Figure S2 (Supporting Information), along with their calculated spectra. These species are considerably higher in energy (1.21 and 1.41 eV) and they have a hydrogen-bonded OH group, giving rise to characteristic very strong vibrations below 3300 cm^{-1}, which are clearly not present in the experimental spectrum.

On the other hand, the calculated spectrum of the bare species shown in Figure 5C agrees well with the experiment. Computational searches yielded three available D_2 tag binding sites: directly on the copper center, on the water, and on the hydroxide. In the case of the 1-D_2 species, the strongest binding site is the copper site with a calculated binding energy of 1498 cm^{-1}. This is substantially larger than the typical value of 370−490 cm^{-1} found for H_2-tagging on protonated peptides.[31] The presence of the D_2 molecule distorts the O−Cu−O bond from linear to bent, as shown in Figure 5B. Nonetheless, the calculated spectrum is not very different from the bare species and is found to be in excellent agreement with the experimental spectrum. This allows us to assign the peak at 3590 cm^{-1} to mostly the hydroxide OH stretch with some contribution from the water symmetric stretch. This is 35 cm^{-1} higher than the vibrational frequency of the isolated hydroxide anion (3555 cm^{-1}),[32] indicated in Figure 5A. The peaks at 3612 and 3684 cm^{-1} are the symmetric and antisymmetric stretches of the water ligand. They are red-shifted with respect to the frequencies of free water (3657 and 3756 cm^{-1}). The weak feature at 3758 cm^{-1} is not present in the calculated spectra. It is most likely a combination band involving the torsional mode and the antisymmetric water stretch, as observed in similar Ar-tagged spectra of $Cu^+(H_2O)$.[17] The weak feature at 2733 cm^{-1} is assigned to the nominally forbidden D_2 stretch which gains intensity from the perturbation induced by binding to the ion.[22,31] It is red-shifted by 261 cm^{-1} from the vibrational frequency of free D_2 at 2994 cm^{-1}.[33] The intensity and position of this transition are reproduced fairly well in the calculated spectrum.

The $CuOH^+\cdot(H_2O)\cdot D_2$ spectrum displays a slowly increasing background starting at ∼2900 cm^{-1} with a dip at ∼3600 cm^{-1}. Similar features are observed on the $CuOH^+\cdot(H_2O)$ species with more D_2 tags (Figure 4), but not in any spectra of the larger $CuOH^+\cdot(H_2O)_n$ clusters. It is unlikely that the dip is due to further dissociation of the $CuOH^+\cdot(H_2O)$ photoproducts because the energy threshold for such process is calculated to be about 1.9 eV. The combination of the background and dip near the peaks is reminiscent of a Fano line shape,[34,35] which is due to a direct coupling between a vibrational mode and the dissociation continuum. It is not clear why this would be operative in the $CuOH^+\cdot(H_2O)$ spectra. The binding energy of the first tag is much larger than usual (and that of the other $CuOH^+\cdot(H_2O)_n$ species discussed below), which brings the dissociation threshold closer to the vibrations, possibly playing a role in the presence of the Fano line shape. However, adequate theoretical treatment of such coupling is outside the scope of the present work.

We can now follow the evolution of the $CuOH^+\cdot(H_2O)$ experimental spectra as a function of increasing number of D_2 tags, shown in Figure 4. The optimized geometries and calculated vibrations at the cam-B3LYP/TZVP level are shown in Figure S3 of the Supporting Information. Calculations found that the second D_2 can bind to either the Cu center or the water ligand with 544 and 361 cm^{-1} binding energy, respectively. It appears that both isomers are present, which would account for the broad appearances of the water modes in Figure 4B. The stepwise filling of these binding sites yields a structure for the 4-D_2 cluster in which two of the D_2 are on the Cu center and one D_2 on each hydrogen of the water ligand. This scenario accounts for the red shifts of the water peaks and the slow and gradual blue shift of the hydroxide stretch as the number of tags increases. Lastly, we note that the good signal-to-noise ratio in the spectrum of the 4-D_2 species reveals three peaks in the 2700−3000 cm^{-1} region. These can be readily

dx.doi.org/10.1021/jp411614t | J. Phys. Chem. A 2014, 118, 2063−2071

assigned to the vibration of the strongly bound first D_2 on copper (2752 cm^{-1}), the weakly bound second D_2 on copper (2921 cm^{-1}), and two weakly bound D_2 on water (2956 cm^{-1}), by comparison with the calculated frequencies (Figure S3, Supporting Information).

The cam-B3LYP/TZVP results for the $CuOH^+\cdot(H_2O)\cdot(D_2)_n$ species showed two noticeable deviations from the experimental spectra, which are particularly visible in the 4-D_2 spectrum. First, the calculated frequency for the D_2-perturbed symmetric water vibration (W−S) is ∼50 cm^{-1} lower than the experimental value. To probe this interaction in more detail, both cam-B3LYP/TZVP and CCSD/TZVP calculations were carried out for the $CuOH^+\cdot(H_2O)\cdot D_2$ cluster in which the D_2 binds to the water ligand (Figure S4 in Supporting Information). The CCSD result yielded a D_2 binding energy of 148 cm^{-1} and a D_2-perturbed W−S vibration at 3561 cm^{-1}. On the other hand, cam-B3LYP yielded a D_2 binding energy of 441 cm^{-1} with a D_2-perturbed W−S vibration at 3450 cm^{-1}. This corroborates the experimental result that cam-B3LYP calculations overestimate the D_2 tag interaction, resulting in an overly red-shifted water vibration. The second deviation is the calculated hydroxide vibration which is ∼15 cm^{-1} higher in frequency than the experimental value in the cam-B3LYP result. This appears to be a systematic error present at all levels of theory because the CCSD result has an even higher frequency for the hydroxide vibration. In the interpretation of the infrared spectra of the larger clusters, these two discrepancies in the calculated spectrum will be considered when assignments are made.

The spectrum of the $CuOH^+\cdot(H_2O)_2\cdot D_2$ cluster in the OH region, displayed in Figure 6A, shows five distinct peaks. The additional feature at 2960 cm^{-1} (Figure 3B) can be readily assigned to the vibration of a weakly bound D_2. This indicates that the strongly interacting Cu-D_2 motif of the n = 1 species is not present here. The cam-B3LYP/TZVP calculation result for the bare $CuOH^+\cdot(H_2O)_2$ is shown in Figure 6E. As expected, the additional water is found where the strongly bound D_2 was in the smaller cluster. This yields a geometry in which hydroxide and the two waters form an almost trigonal planar structure. The two water ligands differ slightly, where one has in-plane hydrogen atoms and one has out-of-plane hydrogen atoms. This causes the two waters to have slightly different vibrational frequencies and binding energies. The waters are labeled W_1 and W_2, which correspond to their clockwise position relative to the hydroxide in the structure displayed throughout Figure 6.

The weakly bound D_2 can bind to the copper center, the water ligand, or the hydroxide ligand, as discussed above. Structure, vibrational frequencies, and binding energies calculated at the cam-B3LYP level for these three isomers are shown in Figure 6B−D. We note that two almost equivalent structures were found for the lowest energy isomer in which the D_2 binds to W_1. They correspond to D_2 binding to either of the two out-of-plane water hydrogens and yield slightly different spectra shown as solid and dashed lines in Figure 6B. Furthermore, all the starting geometries with D_2 on W_2 converged to the same two isomers as in Figure 6B.

Taking into account that the cam-B3LYP calculations overestimate the red shift of the D_2-perturbed W_1-S mode and the frequency of the hydroxyl stretch, we find the calculated spectra of the two isomers in Figure 6B give the best match with the experimental spectrum. Moreover, the slight differences in the vibrational spectra of these two isomers

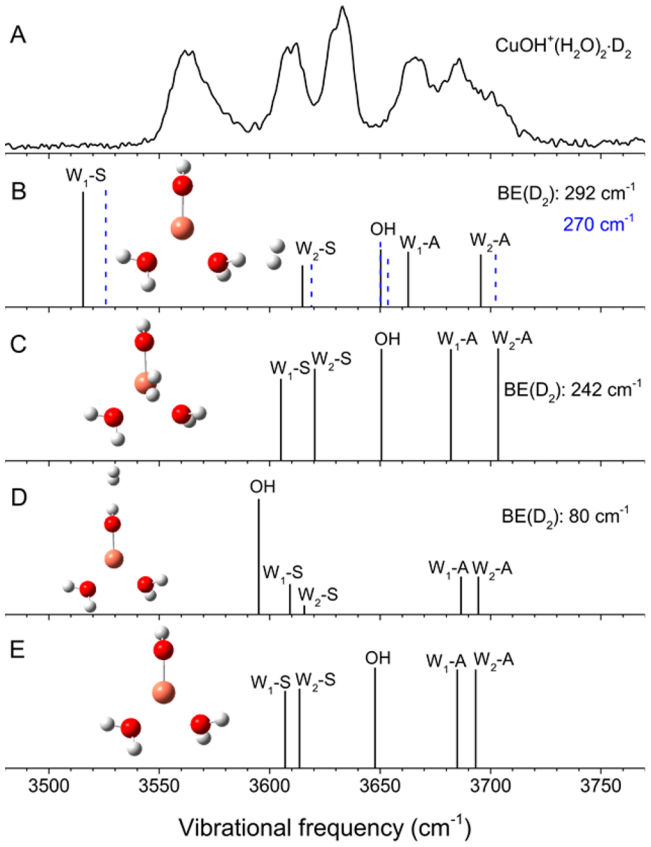

Figure 6. (A) Experimental spectrum of $CuOH^+\cdot(H_2O)_2\cdot D_2$. (B)−(D) Optimized geometries and vibrations calculated at the cam-B3LYP/TZVP level. Shown in blue dashes in (B) are the vibrations corresponding to D_2 binding on the other binding site on the same water. (E) Optimized geometries and vibrations of the untagged cluster. The waters are labeled W_1 and W_2, corresponding to their clockwise position relative to the hydroxide.

would account for the broader and asymmetrical appearance of the features at 3565 and 3685 cm^{-1}. Though the presence of isomers depicted in Figure 6C or 6D cannot be completely ruled out, they are certainly not major contributors because neither reproduces the lowest frequency OH band. Consequently, we make the following assignments: water antisymmetric stretch at 3685 and 3665 cm^{-1}, hydroxide stretch at 3632 cm^{-1}, and water symmetric stretch at 3610 and 3565 cm^{-1}. We note that this assignment, similar to the $CuOH^+\cdot(H_2O)$ clusters, yields an underestimation of ∼50 cm^{-1} for the W_1−S (D_2-bound OH) mode and an overestimation of 18 cm^{-1} for the hydroxide stretch in the cam-B3LYP calculation.

There may be a couple of reasons why the isomer in Figure 6B dominates the experimental spectrum. First, the calculations indicate it is the lowest energy isomer. Even though isomers 6c and 6d are not significantly higher in energy, the potential energy surface is likely quite flat, allowing the clusters to reach the lowest energy isomer during collisional cooling. Furthermore, there are four almost equivalent binding sites for D_2 on the water ligand, whereas there is only one binding site on hydroxide and at most two on copper. Therefore, the isomer in Figure 6B is also favored from a statistical point of view.

We now turn our attention to the larger $CuOH^+\cdot(H_2O)_3$ cluster. If the additional water bonds to another water molecule and forms a second solvation shell, it would give rise to the

dx.doi.org/10.1021/jp411614t | J. Phys. Chem. A 2014, 118, 2063−2071

typical H-bonded water transitions in the 3100−3400 cm^{-1} region.[18,36] No feature in that range is observed in the experimental spectrum of the $n = 3$ cluster. Therefore, the $n = 3$ cluster has three waters and a hydroxide group on the copper center. The cam-B3LYP calculations produced a cluster with an almost square planar geometry, shown in Figure 7D along with

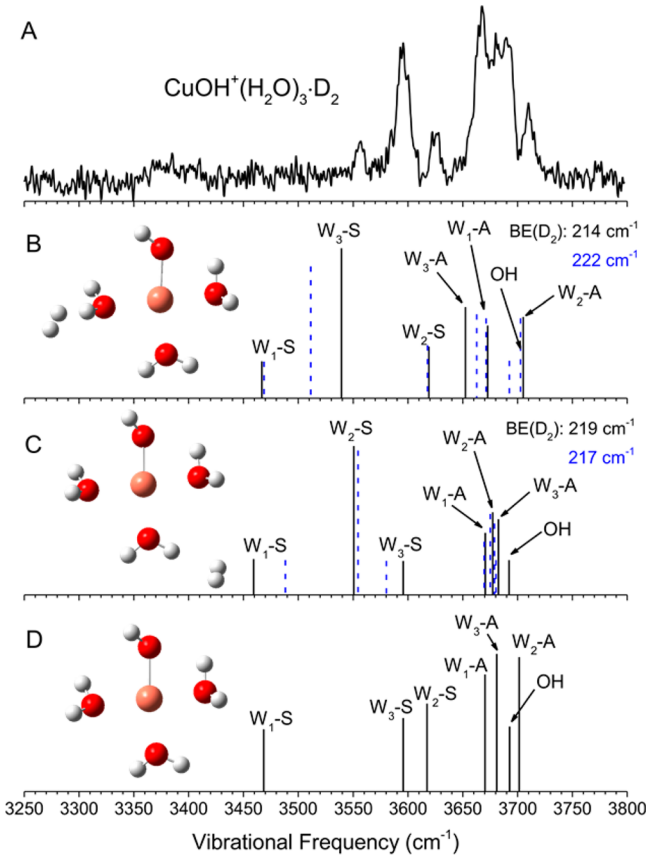

Figure 7. (A) Experimental spectrum of $CuOH^+\cdot(H_2O)_3\cdot D_2$. (B) and (C) Optimized geometries and vibrations calculated at the cam-B3LYP level. Shown in blue dashes are the vibrations corresponding to D_2 binding on the other binding site on the same water. (D) Optimized geometries and vibrations of the untagged cluster.

its infrared spectrum. We again used the same W_1, W_2, and W_3 labeling, corresponding to the clockwise position starting from hydroxide. The arrangement of the ligands around the copper center is more akin to $Cu^{2+}(H_2O)_n$[12,20] than $Cu^+(H_2O)_n$[19] in which only two water molecules are present in the primary solvation shell. The hydroxide acts as a slight hydrogen bond acceptor for the neighboring W_1 water, which distorts the ligand arrangement and yields three nonequivalent waters.

Again, we found that D_2 binding to water gives the lowest energy structures. Because the $CuOH^+\cdot(H_2O)_2$ cluster showed only contributions from this binding site, we will only consider these D_2 binding isomers in detail here. The cam-B3LYP calculations yielded four possible D_2 tag isomers, in which D_2 binds to W_2 (Figure 7C) or W_3 (Figure 7B). Starting geometries with D_2 on W_1 all produced rearrangements leading to the structure in Figure 7B. As expected, the calculated D_2 binding energies for all the species are essentially the same. However, none of the calculated spectra present a very good match with the experiment. The best agreement comes from isomer in Figure 7B (solid black lines), if we use the same calibrations for the calculated frequency as before. We can assume that the frequency of the hydroxide is once again overestimated by ∼15 cm^{-1} and the frequency of the D_2-bound W_3-S is underestimated by ∼50 cm^{-1}. This yields a good agreement for the six highest frequency peaks with the following assignments: water antisymmetric stretch at 3710, 3681, and 3667 cm^{-1}, hydroxide stretch at 3692 cm^{-1}, and water symmetric stretch at 3625 and 3595 cm^{-1}. This only leaves the small peak at 3556 cm^{-1} to be the W_1-S peak, calculated to be 90 cm^{-1} lower in frequency. This vibration is red-shifted due to W_1 forming a hydrogen bond donor interaction with the nearby oxygen of the hydroxide. It is conceivable that, similar to the D_2 binding induced shift, the calculations overestimate the effect of this interaction in the infrared spectrum. Although the presence of the other isomers cannot be completely ruled out, the narrow 10 cm^{-1} fwhm of all the peaks indicates that a single isomer is probably responsible for all the features in the experimental spectrum.

From the assigned spectra, we can see some interesting trends in the evolution of the clusters. First, the hydroxide stretch blue shifts by ∼100 cm^{-1} with increasing number of water ligands, moving from 3590 cm^{-1} in $n = 1$ to 3692 cm^{-1} in $n = 3$. A similar trend, but of smaller magnitude, is also observed in the spectra of $CuOH^+\cdot(H_2O)\cdot(D_2)_n$ in which the hydroxide peak shifts from 3590 to 3609 cm^{-1} as the number of D_2 tags is increased. Interestingly, the hydroxide vibration for the smallest cluster studied here is already at a higher frequency than either the isolated hydroxyl radical (3570 cm^{-1}) or hydroxide anion (3555 cm^{-1}). In fact, as solvation increases around the Cu center, this vibration is moving toward the typical frequency of a free OH in water or alcohol (∼3700 cm^{-1}).[37] This can be seen in Figure 3C, where the hydroxide stretch is only 18 cm^{-1} lower in frequency than the antisymmetric stretch of the "free" water in the $n = 3$ cluster. Very similar behavior of the hydroxide mode has been observed before in the infrared spectra of small $OH^-(H_2O)_n$ clusters.[38] On the other hand, the vibrational frequencies of the "free" water ligand, i.e., not hydrogen-bonded or D_2-bonded, are much less sensitive to the increasing solvation. These modes show almost no shift from $n = 1$ (3612/3684 cm^{-1}) to $n = 2$ (3610/3685 cm^{-1}), but slightly blue shifts in $n = 3$ (3625/3710 cm^{-1}), moving closer to the gas phase H_2O vibrations (3657/3756 cm^{-1}). The calculation at the cam-B3LYP level yielded incremental water binding energies of 2.18, 1.26, and 0.94 eV for the first, second, and third water, respectively. The red shift of the free water ligand is thus not directly related to the binding energy. A possible explanation is that the vibrational frequency shift is mostly due to the electric field induced by the charged $CuOH^+$ ion core.[39]

Although the copper center in the clusters studied here has a formal oxidation state of +2, NBO analysis determined that the copper center has a charge varying from +1.05 to +1.14 as the number of water increases. This is not surprising considering that the ionic charge-separated state is likely to be much higher in energy for these small clusters. However, the square planar arrangement of the ligands around the copper center found in this work is similar to $Cu^{2+}(H_2O)_n$[12,20] and not $Cu^+(H_2O)_n$[19] in which only two water molecules are present in the primary solvation shell. Although the second and third water have significantly lower binding energies than the first water, it is not sufficient to force them into the second solvation shell. We did not observe any significant intensity in the mass spectrum for clusters containing more than three water ligands. This

dx.doi.org/10.1021/jp411614t | J. Phys. Chem. A 2014, 118, 2063−2071

indicates that the fourth water, whether binding on the axial Cu site or hydrogen bonding to the primary water ligand, has a much lower binding energy. The closure of the first solvation shell at three waters would be consistent with the square planar coordination observed for the $Cu^{2+}(H_2O)_n$ clusters.

The well-resolved spectra afforded by the cryogenic ion vibrational spectroscopy technique have enabled us to point out some subtle discrepancies between the cam-B3LYP calculated spectrum and the experimental results. We briefly studied the effects of different calculation methods to explore the origin of these discrepancies. We found that the calculated structures and vibrational spectra were very dependent on the calculation method. An example of this is shown in Figure 8, which

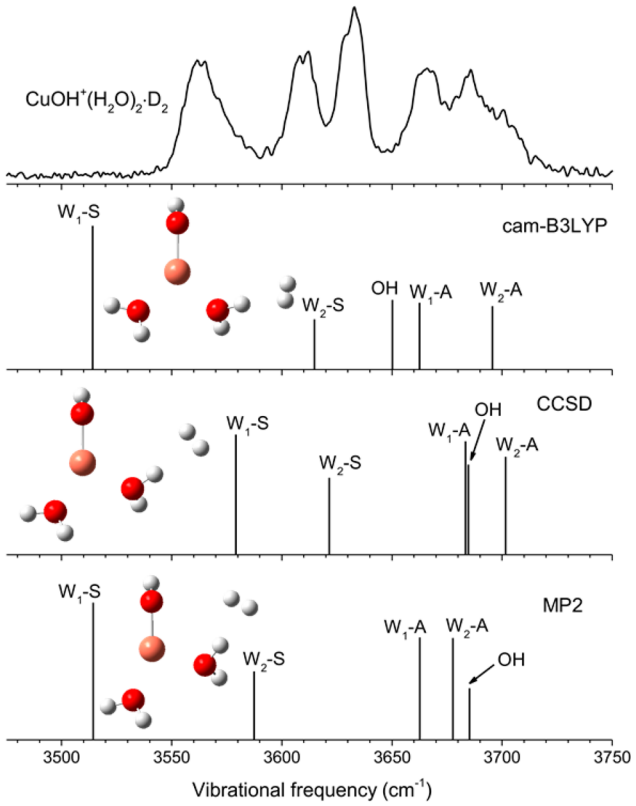

Figure 8. Comparison of the calculation results at cam-B3LYP, MP2, and CCSD levels with experimental result.

compares the structures and spectra of the $CuOH^+·(H_2O)_2·D_2$ cluster at the cam-B3LYP, MP2, and CCSD methods using the same TZVP basis set. As discussed before, the cam-B3LYP calculation gives a geometry close to a trigonal planar ligand arrangement for this species. On the other hand, MP2 yields an almost T-shaped geometry, whereas the CCSD result is somewhere between the two. In assigning the experimental spectra, we noted that cam-B3LYP calculations consistently overestimate the hydroxide frequency by ~15 cm^{-1}. Interestingly, both MP2 and CCSD, with a more T-shaped geometry, yielded a hydroxide mode ~35 cm^{-1} higher than the cam-B3LYP calculation. This suggests that the geometry for the n = 2 cluster might be even closer to symmetrically trigonal planar than predicted by cam-B3LYP. However, whereas cam-B3LYP may be closest in obtaining the correct hydroxide frequency, it fails in predicting the correct interaction strength for both the D_2–H_2O interaction and the slight hydrogen bond in the n = 3 cluster. The CCSD calculation is better at accounting for these weak intermolecular interactions despite not having the right geometry. The cause of these method dependent geometries is not clear. One possibility is the open-shell nature of these Cu complexes, which can cause spin-contamination problems. However, in the case of the calculations shown in Figure 8, we found S^2 to be very close to the expected 0.75 value (0.758 for cam-B3LYP, and 0.754 for MP2 and CCSD). Furthermore, the T-shaped MP2 structure is closer to the linear coordination expected for Cu^+ centers. This suggests that differences between the various calculation methods might stem from the different treatment of charge transfer between the Cu^{2+} center and the OH^- ligand.

We note that similar method dependent geometries have previously been reported for other Cu complexes. Wang et al.[40] have reported significantly different geometries for Cu-(2,2′-bipyridine) and Cu-(4,4′-bipyridine) complexes calculated using MP2 and B3LYP. Comparison with high resolution photoelectron spectra indicated that the structure of Cu-(2,2′-bipyridine) was correctly predicted by B3LYP whereas the structure of Cu-(4,4′-bipyridine) was best described by MP2. Rios-Font et al.[41] have also found significant effects by the amount of exact exchange in DFT functional for the description of $Cu^{2+}(H_2O)_n$ water clusters.

V. CONCLUSION

The $CuOH^+·(H_2O)_n$ (n = 1–3) clusters were isolated using electrospray ionization and studied by cryogenic ion vibrational spectroscopy. The resolution afforded in the OH region allowed for a detailed analysis and assignment of the experimental spectra. The results showed that the copper center in the $CuOH^+·(H_2O)_3$ cluster has a distorted square planar geometry. The coordination in $CuOH^+·(H_2O)_n$ is found to be more akin to $Cu^{2+}(H_2O)_n$ with four ligands in the first solvation shell than $Cu^+(H_2O)_n$ with two ligands in the first solvation shell. The undercoordinated $CuOH^+·(H_2O)$ cluster showed a high reactivity, binding strongly to the D_2 tag and significantly shifting the D_2 stretch. The larger $CuOH^+·(H_2O)_2$ and $CuOH^+·(H_2O)_3$ clusters did not show such a strong interaction. The well-resolved spectra also enabled us to point out some discrepancies between the calculated spectra and the experimental results, which were found to be highly dependent on the level of theory used. Care is needed for proper simulation of the coordinated copper complexes.

■ ASSOCIATED CONTENT

Supporting Information

Mass spectra when the photodissociation laser is on/off resonance (Figure S1), calculated geometries and vibrational spectra for higher energy isomers of the n = 1 species (Figure S2), comparison of the experimental and calculated spectra of the n = 1 species with 1–4 D_2 tags (Figure S3), comparison of cam-B3LYP and CCSD methods for D_2-water interaction (Figure S4), and the complete ref 30 are presented in the Supporting Information. This information is available free of charge via the Internet at http://pubs.acs.org

■ AUTHOR INFORMATION

Corresponding Author

*E. Garand: e-mail, egarand@chem.wisc.edu.

Notes

The authors declare no competing financial interest.

■ ACKNOWLEDGMENTS

The authors acknowledge the Donors of the American Chemical Society Petroleum Research Fund for partial support of this research. The experimental setup used in this study was built using start-up funds from the UW Madison chemistry department. The computational resources used in this work are supported by National Science Foundation Grant CHE-0840494.

■ REFERENCES

(1) Wendlandt, A. E.; Suess, A. M.; Stahl, S. S. Copper-Catalyzed Aerobic Oxidative C-H Functionalizations: Trends and Mechanistic Insights. *Angew. Chem.-Int. Ed.* **2011**, *50*, 11062−11087.
(2) Chen, Z. F.; Meyer, T. J. Copper(II) Catalysis of Water Oxidation. *Angew. Chem.-Int. Ed.* **2013**, *52*, 700−703.
(3) Zhang, M. T.; Chen, Z. F.; Kang, P.; Meyer, T. J. Electrocatalytic Water Oxidation with a Copper(II) Polypeptide Complex. *J. Am. Chem. Soc.* **2013**, *135*, 2048−2051.
(4) Barnett, S. M.; Goldberg, K. I.; Mayer, J. M. A Soluble Copper-Bipyridine Water-Oxidation Electrocatalyst. *Nat. Chem.* **2012**, *4*, 498−502.
(5) Chen, Z. F.; Kang, P.; Zhang, M. T.; Stoner, B. R.; Meyer, T. J. Cu(II)/Cu(0) Electrocatalyzed CO_2 and H_2O Splitting. *Energy Environ. Sci.* **2013**, *6*, 813−817.
(6) Asmis, K. R.; Neumark, D. M. Vibrational Spectroscopy of Microhydrated Conjugate Base Anions. *Acc. Chem. Res.* **2012**, *45*, 43−52.
(7) Dopfer, O. IR Spectroscopy of Microsolvated Aromatic Cluster Ions: Ionization-Induced Switch in Aromatic Molecule-Solvent Recognition. *Z. Phys. Chem.* **2005**, *219*, 125−168.
(8) Duncan, M. A. Infrared Spectroscopy to Probe Structure and Dynamics in Metal Ion−Molecule Complexes. *Int. Rev. Phys. Chem.* **2003**, *22*, 407−435.
(9) Polfer, N. C.; Oomens, J. Vibrational Spectroscopy of Bare and Solvated Ionic Complexes of Biological Relevance. *Mass Spectrom. Rev.* **2009**, *28*, 468−494.
(10) Dalleska, N. F.; Honma, K.; Sunderlin, L. S.; Armentrout, P. B. Solvation of Transition-Metal Ions by Water - Sequential Binding-Energies of $M^+(H_2O)_x$, (x=1−4) for M=Ti to Cu Determined by Collision-Induced Dissociation. *J. Am. Chem. Soc.* **1994**, *116*, 3519−3528.
(11) Magnera, T. F.; David, D. E.; Stulik, D.; Orth, R. G.; Jonkman, H. T.; Michl, J. Production of Hydrated Metal-Ions by Fast Ion or Atom Beam Sputtering - Collision-Induced Dissociation and Successive Hydration Energies of Gaseous Cu^+ with 1−4 Water-Molecules. *J. Am. Chem. Soc.* **1989**, *111*, 5036−5043.
(12) Duncombe, B. J.; Duale, K.; Buchanan-Smith, A.; Stace, A. J. The Solvation of Cu^{2+} with Gas-Phase Clusters of Water and Ammonia. *J. Phys. Chem. A* **2007**, *111*, 5158−5165.
(13) Stace, A. J.; Walker, N. R.; Firth, S. $Cu(H_2O)_n^{2+}$ Clusters: The First Evidence of Aqueous Cu(II) in the Gas Phase. *J. Am. Chem. Soc.* **1997**, *119*, 10239−10240.
(14) Shvartsburg, A. A.; Siu, K. W. M. Is There a Minimum Size for Aqueous Doubly Charged Metal Cations? *J. Am. Chem. Soc.* **2001**, *123*, 10071−10075.
(15) Stone, J. A.; Vukomanovic, D. Collisional Dissociation Studies of $Cu^{2+}(H_2O)_n$ Using Electrospray Ionization Mass Spectrometry. *Int. J. Mass Spectrom.* **1999**, *185*, 227−229.
(16) Vukomanovic, D.; Stone, J. A. A Low-Energy CAD Study of the Ions $MOH(H_2O)^+$ (M = Mn, Co, Ni, Cu, Zn) and $M(H\text{-}2,O\text{-}2)^+$ (M = Cr, Fe, La, Pr). *Int. J. Mass Spectrom.* **2000**, *202*, 251−259.
(17) Carnegie, P. D.; McCoy, A. B.; Duncan, M. A. IR Spectroscopy and Theory of $Cu^+(H_2O)Ar_2$ and $Cu^+(D_2O)Ar_2$ in the O-H (O-D) Stretching Region: Fundamentals and Combination Bands. *J. Phys. Chem. A* **2009**, *113*, 4849−4854.
(18) Iino, T.; Ohashi, K.; Inoue, K.; Judai, K.; Nishi, N.; Sekiya, H., Infrared Spectroscopy of $Cu^+(H_2O)_n$ and $Ag^+(H_2O)_n$: Coordination and Solvation of Noble-Metal Ions. *J. Chem. Phys.* **2007**, *126*.
(19) Iino, T.; Ohashi, K.; Mune, Y.; Inokuchi, Y.; Judai, K.; Nishi, N.; Sekiya, H. Infrared Photodissociation Spectra and Solvation Structures of $Cu^+(H_2O)_n$ (n=1−4). *Chem. Phys. Lett.* **2006**, *427*, 24−28.
(20) O'Brien, J. T.; Williams, E. R. Hydration of Gaseous Copper Dications Probed by IR Action Spectroscopy. *J. Phys. Chem. A* **2008**, *112*, 5893−5901.
(21) Robertson, W. H.; Johnson, M. A. Molecular Aspects of Halide Ion Hydration: The Cluster Approach. *Annu. Rev. Phys. Chem.* **2003**, *54*, 173−213.
(22) Kamrath, M. Z.; Relph, R. A.; Guasco, T. L.; Leavitt, C. M.; Johnson, M. A. Vibrational Predissociation Spectroscopy of the H_2-Tagged Mono- and Dicarboxylate Anions of Dodecanedioic Acid. *Int. J. Mass Spectrom.* **2011**, *300*, 91−98.
(23) Fenn, J. B.; Mann, M.; Meng, C. K.; Wong, S. F.; Whitehouse, C. M. Electrospray Ionization for Mass-Spectrometry of Large Biomolecules. *Science* **1989**, *246*, 64−71.
(24) Fenn, J. B.; Mann, M.; Meng, C. K.; Wong, S. F.; Whitehouse, C. M. Electrospray Ionization-Principles and Pratice. *Mass Spectrom. Rev.* **1990**, *9*, 37−70.
(25) Hock, C.; Kim, J. B.; Weichman, M. L.; Yacovitch, T. I.; Neumark, D. M., Slow Photoelectron Velocity-Map Imaging Spectroscopy of Cold Negative Ions. *J. Chem. Phys.* **2012**, *137*.
(26) Wang, X. B.; Wang, L. S., Development of a Low-Temperature Photoelectron Spectroscopy Instrument Using an Electrospray Ion Source and a Cryogenically Controlled Ion Trap. *Rev. Sci. Instrum.* **2008**, *79*.
(27) Johnson, M. A.; Alexander, M. L.; Lineberger, W. C. Photodestruction Cross-Sections for Mass-Selected Ion Clusters - $(CO_2)_N^+$. *Chem. Phys. Lett.* **1984**, *112*, 285−290.
(28) Mathur, R.; O'Connor, P. B. Design and Implementation of a High Power RF Oscillator on a Printed Circuit Board for Multipole Ion Guides. *Rev. Sci. Instrum.* **2006**, *77*.
(29) O'Connor, P. B.; Costello, C. E.; Earle, W. E. A High Voltage RF Oscillator for Driving Multipole Ion Guides. *J. Am. Soc. Mass Spectrom.* **2002**, *13*, 1370−1375.
(30) Frisch, M. J.; Trucks, G. W.; Schlegel, H. B.; Scuseria, G. E.; Robb, M. A.; Cheeseman, J. R.; Scalmani, G.; Barone, V.; Mennucci, B.; Petersson, G. A.; et al. *Gaussian 09*; Gaussian, Inc.: Wallingford, CT, 2009.
(31) Kamrath, M. Z.; Garand, E.; Jordan, P. A.; Leavitt, C. M.; Wolk, A. B.; Van Stipdonk, M. J.; Miller, S. J.; Johnson, M. A. Vibrational Characterization of Simple Peptides Using Cryogenic Infrared Photodissociation of H_2-Tagged, Mass-Selected Ions. *J. Am. Chem. Soc.* **2011**, *133*, 6440−6448.
(32) Rosenbaum, N. H.; Owrutsky, J. C.; Tack, L. M.; Saykally, R. J. Velocity Modulation Laser Spectroscopy of Negative-Ions - The Infrared-Spectrum of Hydroxide (OH-). *J. Chem. Phys.* **1986**, *84*, 5308−5313.
(33) Dickenson, G. D.; Niu, M. L.; Salumbides, E. J.; Komasa, J.; Eikema, K. S. E.; Pachucki, K.; Ubachs, W. Fundamental Vibration of Molecular Hydrogen. *Phys. Rev. Lett.* **2013**, *110*.
(34) Fano, U. Effects of Configuration Interaction on Intensities and Phase Shifts. *Phys. Rev.* **1961**, *124*, 1866−1878.
(35) Fano, U.; Cooper, J. W. Line Profiles in Far-UV Absorption Spectra of Rare Gases. *Phys. Rev.* **1965**, *137*, 1364−&.
(36) Bandyopadhyay, B.; Reishus, K. N.; Duncan, M. A. Infrared Spectroscopy of Solvation in Small $Zn^+(H_2O)_n$ Complexes. *J. Phys. Chem. A* **2013**, *117*, 7794−7803.
(37) Shin, J. W.; Hammer, N. I.; Diken, E. G.; Johnson, M. A.; Walters, R. S.; Jaeger, T. D.; Duncan, M. A.; Christie, R. A.; Jordan, K. D. Infrared Signature of Structures Associated with the $H^+(H_2O)_n$ (n=6 to 27) Clusters. *Science* **2004**, *304*, 1137−1140.
(38) Robertson, W. H.; Diken, E. G.; Price, E. A.; Shin, J. W.; Johnson, M. A. Spectroscopic Determination of the OH^- Solvation Shell in the $OH^-(H_2O)_n$ clusters. *Science* **2003**, *299*, 1367−1372.
(39) Prell, J. S.; O'Brien, J. T.; Williams, E. R. Structural and Electric Field Effects of Ions in Aqueous Nanodrops. *J. Am. Chem. Soc.* **2011**, *133*, 4810−4818.

(40) Wang, X.; Lee, J. S.; Yang, D.-S. High-Resolution Electron Spectroscopy and Molecular Structures of Cu-(2,2 ′-bipyridine) and Cu-(4,4 ′-bipyridine). *Can. J. Chem.* **2013**, *91*, 613−620.
(41) Rios-Font, R.; Sodupe, M.; Rodriguez-Santiago, L.; Taylor, P. R. The Role of Exact Exchange in the Description of $Cu^{2+}(H_2O)_n$ (n=1−6) Complexes by Means of DFT Methods. *J. Phys. Chem. A* **2010**, *114*, 10857−10863.